Achieving complete columnar-to-equiaxed transition in laser-processed AlCoCrFeNi alloys via mixed powder preparation

Scripta Materialia 277 (2026) 117223

Contents lists available at ScienceDirect

Scripta Materialia

journal homepage: www.journals.elsevier.com/scripta-materialia

Achieving complete columnar-to-equiaxed transition in laser-processed AlCoCrFeNi alloys via mixed powder preparation

Hui Zhang [a], Yuyun Lu [a], Xueting Wu [b], Jingxi Zhang [c], Dong Hao [a], Ye Tao [a], Lei Hu [a], Dongzhen Qi [a], Kaio Niitsu Campo [d,*], Sheng Guo [e,*]

[a] School of Materials Science and Engineering, Anhui University of Technology, Ma'anshan 243002, Anhui, , China
[b] School of Materials and Environmental Engineering, Chizhou University, Chizhou 247000, Anhui, China
[c] School of Mechanical Engineering, Shandong University of Technology, Zibo 255000, Shandong, China
[d] School of Mechanical Engineering, University of Campinas, Campinas, SP 13083-860, Brazil
[e] Department of Industrial and Materials Science, Chalmers University of Technology SE-41296, Gothenburg, Sweden

ARTICLE INFO

Keywords:
High-entropy alloys
Laser processing
Columnar-to-equiaxed transition
Mechanically mixed powders

ABSTRACT

The columnar-to-equiaxed transition (CET) is critical for mitigating microstructural anisotropy and intergranular cracking associated with columnar grains in laser-processed alloys. Here, a complete CET was achieved in an AlCoCrFeNi high-entropy alloy using mechanically mixed powders, resulting in more than an order-of-magnitude grain refinement compared with that prepared from pre-alloyed powder. The CET is attributed to liquid-phase undercooling induced by constitutional fluctuations. In this framework, a local inversion of the chemical profile (relative to the normal segregation pattern) ahead of the solid–liquid interface reduces the local liquidus temperature, favoring nucleation over growth, even under the steep thermal gradients inherent to laser processing. While direct observation of liquid compositional fluctuations is not feasible, the proposed mechanism provides a physically consistent explanation for the experimental observations. These findings suggest a new pathway for microstructural control in laser processing, where engineered compositional fluctuations may be exploited to tailor grain structures in multicomponent alloys.

Laser processing of high-entropy alloys (HEAs) represents a prominent research area owing to its potential to optimize microstructural characteristics and enhance overall performance [1]. For example, Ren et al. fabricated a nano-lamellar $AlCoCrFeNi_{2.1}$ HEA using laser additive manufacturing (LAM), achieving a synergy of strength and ductility, with a yield strength of 1.3 GPa and 14 % elongation [2]. Similarly, Shittu et al. found that the tribo-corrosion rate of LAM-fabricated CoCrFeMnNi in 3.5 wt. % NaCl was six times lower than that of the same alloy prepared by arc melting [3]. However, columnar grains are typically unavoidable in laser melt pools due to large temperature gradients (G), leading to anisotropic properties and increased susceptibility to intergranular cracking [4].

Therefore, many researchers have focused on achieving a complete columnar-to-equiaxed transition (CET) by tailoring the solidification rate (R) and G through laser parameters control, as well as by optimizing alloy composition to enhance constitutional undercooling [5,6]. As early as 40 years ago, Hunt developed the classical CET model, demonstrating that constitutional undercooling ahead of the columnar front increases nucleation and promotes CET as the G/R ratio decreases with solidification [7]. This theoretical framework provides a basis for understanding the transition observed in laser melt pools under specific conditions, where columnar grains at the bottom evolve into equiaxed grains toward the top [8].

Alloys with higher solute contents are generally more prone to equiaxed solidification [9]. Recent studies suggest that interactions among multiple solutes can produce synergistic effects on CET. To describe microstructural formation and guide alloy design, empirical and semi-empirical parameters are widely employed, particularly the constitutional supercooling parameter ($P = mC_0(k-1)/k$) and the growth restriction factor ($Q = mC_0(k-1)$), where m is the liquidus slope, C_0 the alloy composition, and k the partition coefficient [10–13]. Higher values of these parameters indicate a greater capacity for constitutional undercooling. Chang et al. observed fully equiaxed grains in a Ti-3Al-6Fe-6V-2Zr (wt. %) alloy, attributing this behavior to Fe addition, which exhibits the highest Q value per unit mass among the available β-eutectoid solutes [14]. Wang et al. utilized a combination of

* Corresponding authors.
E-mail addresses: kaionc@unicamp.br (K.N. Campo), sheng.guo@chalmers.se (S. Guo).

https://doi.org/10.1016/j.scriptamat.2026.117223
Received 5 November 2025; Received in revised form 8 February 2026; Accepted 9 February 2026
Available online 14 February 2026

growth-restricting solutes (Ni and B) to refine prior-β grains in as-printed Ti alloys, promoting an equiaxed α-Ti microstructure with reduced mechanical anisotropy and good tensile properties [15]. Nonetheless, the extremely high G in laser melt pools (10^5–10^7 K/m) [16,17] remains a major obstacle to CET, making it even more difficult to obtain fully equiaxed grains. This remains true even for alloys whose compositions would otherwise favor CET based on their elevated Q values, thus necessitating the use of inoculants for effective microstructural refinement [18,19].

This work demonstrates that laser-processed AlCoCrFeNi can exhibit either columnar or fully equiaxed microstructures, depending on the compositional uniformity of the starting powders. Liquid constitutional fluctuation may serve as a critical factor triggering the CET mechanism, providing a simple yet effective strategy for microstructural refinement. Importantly, this approach can overcome the limitations imposed by the elevated G inherent to laser processing, offering a promising route to enhanced mechanical properties in HEAs.

The AlCoCrFeNi HEA was prepared using two powder types: a mechanically mixed elemental powder blend (in-situ alloying) and a gas-atomized pre-alloyed powder. Powder details are provided in the Supplementary Information. Both powders were laser cladded on low-carbon Q235 steel using identical parameters: 2.4 kW laser power, 4 mm spot size, and 8 mm/s scanning speed. Hereafter, the clad derived from the pre-alloyed powder is referred to GP-HEA, and that from the mechanically mixed powder as MP-HEA. Samples were characterized by optical microscope (Zeiss Axio Vert.A1), X-ray diffractometer (XRD, Bruker D8 Advance) with Cu-Kα radiation, and field-emission gun scanning electron microscope (FEG-SEM, Quanta-450) equipped with electron backscatter diffraction (EBSD) and energy dispersive spectroscopy (EDS) detectors. Scheil curves were obtained using Thermo-Calc® with the TCFE12 database.

Figures 1(a-b) compare the two powder types. The pre-alloyed powder (Fig. 1a) displays high compositional uniformity, with spherical particles of 50–110 μm. In contrast, the mechanically mixed powder contains spherical and near-spherical particles of different elements with notable size differences: larger particles are distinctly visible, while smaller particles form a densely packed, interconnected structure in which individual shapes are hardly discernible. The overall compositions of the laser-processed HEAs are presented in Table 1. While the clads exhibit similar compositions, the Fe content is higher than the nominal value due to substrate dilution. The XRD patterns (Fig. 1c) indicate identical phases in both conditions, consisting of a mixture of BCC and ordered B2 structures. The (100) superlattice reflection confirms B2 ordering, consistent with reports that Al, Co, and Ni occupy

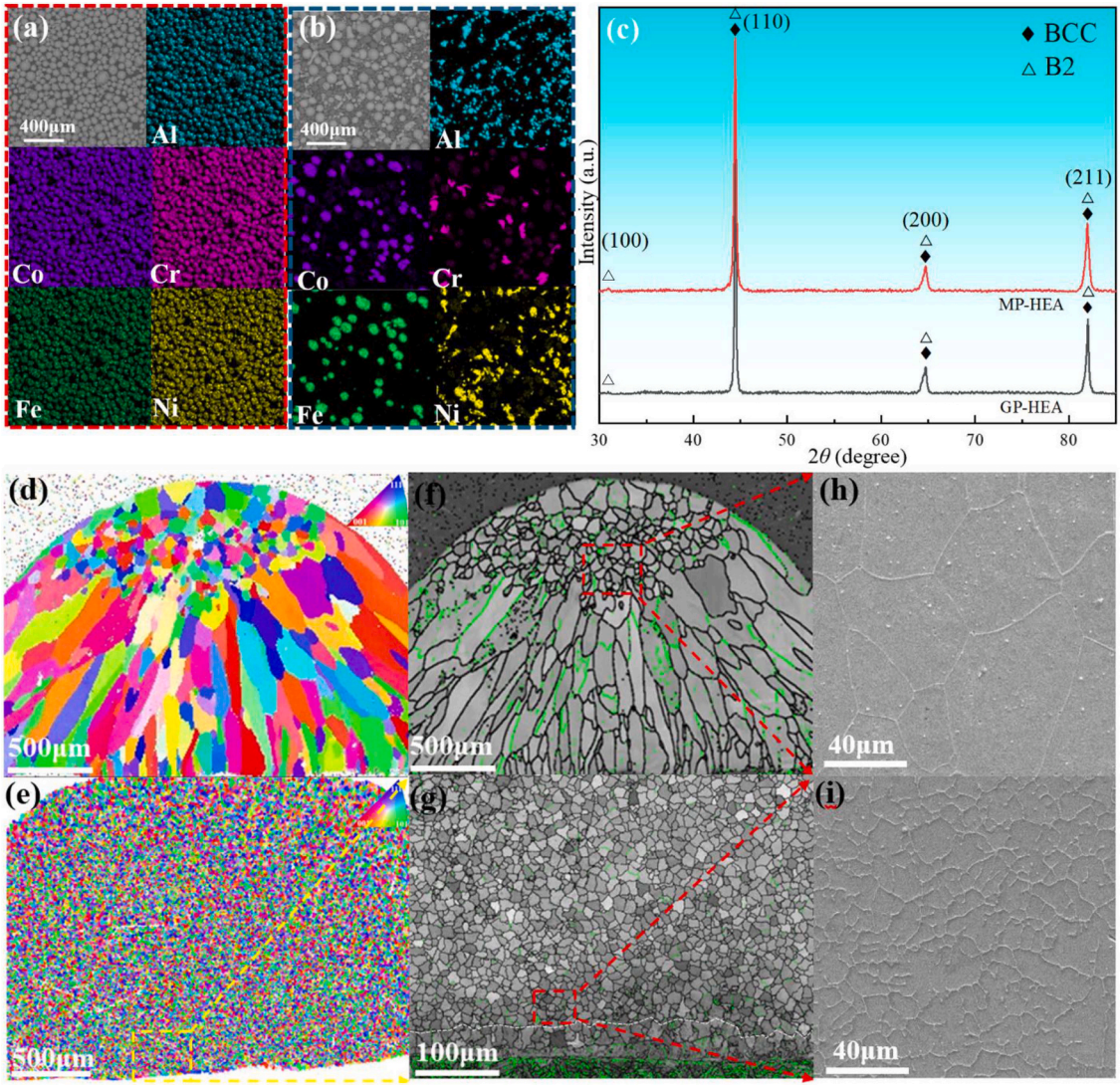

Fig. 1. Morphology and compositional distribution of (a) gas-atomized and (b) mechanically mixed powders. (c) XRD patterns of AlCoCrFeNi HEAs after laser cladding. Cross-sectional EBSD and SEM microstructures of the as-solidified (d, f, h) GP-HEA and (e, g, i) MP-HEA: (d-e) inverse pole figure maps; (f-g) grain boundary maps (black and green lines indicate high- and low-angle boundaries, respectively); (h-i) secondary-electron SEM images.

Table 1
Overall chemical compositions of the as-solidified GP-HEA and MP-HEA determined by SEM-EDS.

Sample	Composition (at. %)				
	Al	Co	Cr	Fe	Ni
GP-HEA	16.21	16.45	16.60	34.59	16.15
MP-HEA	15.37	15.61	16.00	37.71	15.30
Nominal	20	20	20	20	20

specific lattice sites within the BCC lattice [20,21].

Figures 1(d-e) show cross-sectional EBSD microstructures of the as-solidified samples. The GP-HEA predominantly exhibits coarse columnar grains aligned with the heat dissipation direction, with an average width of ~100 μm and length of ~500 μm. In contrast, the MP-HEA consists entirely of refined equiaxed grains, with a characteristic grain size roughly one-tenth that of the GP-HEA. As shown in Fig. 1f, numerous low-angle boundaries (misorientation <15°, green) are distributed within the columnar grains of the GP-HEA, while Fig. 1*g* reveals that equiaxed grains in the MP-HEA are primarily bounded by high-angle boundaries (>15°, black), confirming independent nucleation. A slight grain-size reduction is observed in the MP-HEA from top to bottom (Fig. 1e), with the average equivalent diameter decreasing from ~22 μm to ~18 μm (Fig. S2 in the Supplementary Information). SEM images (Figs. 1(h-i)) further confirm a grain refinement in the MP-HEA exceeding one order of magnitude when benchmarked with the GP-HEA.

The observed microstructure challenges the conventional understanding that CET is primarily governed by bulk composition or laser parameters. It could be argued that oxide particles acted as heterogeneous nucleation sites. However, both powders exhibited similar initial oxygen contents (see Supplementary Information). Although oxide formation has been reported in AlCoCrFeNi-based HEAs, such oxides were not found to induce grain refinement during in-situ solidification experiments [22]. Moreover, if oxides played a dominant role in nucleation, some grain refinement would also be expected in the GP-HEA, which was not observed.

In this study, liquid constitutional fluctuations caused by incomplete powder mixing within the transient laser melt pool are inferred to trigger a full CET. Spatial variations in liquid composition (C_L) shift the local liquidus temperature (T_L), generating irregular constitutional undercooling. Consequently, the advancing *S/L* interface may encounter locally undercooled regions that favor solid growth, or locally overheated regions due to solute profile inversions that momentarily impede its advancement.

For simplicity, consider a liquid with compositional fluctuations schematically shown in Fig. 2a, where two regions with different solidification temperatures are uniformly distributed. These regions, termed higher-temperature liquid ($C_{HT\text{-}L}$) and lower-temperature liquid ($C_{LT\text{-}L}$), coexist prior to solidification. Solidification initiates within $C_{HT\text{-}L}$, with grains growing parallel and opposite to the heat flow direction. As the *S/L* interface advances, it eventually encounters $C_{LT\text{-}L}$ regions with lower solidification temperatures, reducing the growth rate, which is proportional to local undercooling [23], and potentially arresting growth if the local T_L drops below the actual temperature (T_{Actual}). Fig. 2a also depicts this behavior, showing compositional variations and corresponding T_L along line a–a′, together with the steep thermal gradient inherent to laser processing [18].

Although the *S/L* interface is slowed or temporarily suppressed, heat extraction continues, creating a lag between the actual interface position and that predicted by the laser scanning speed, analogous to the discrepancy between growth and pull rates in directional solidification (Bridgman) experiments [19,24]. This lag induces substantial thermal undercooling (ΔT_t) in a $C_{HT\text{-}L}$ region located beyond the $C_{LT\text{-}L}$ zone ahead of the interface. Such undercooling promotes nucleation when the local undercooling (ΔT) exceeds the critical nucleation undercooling (ΔT_n), as illustrated in Fig. 2b In other words, nucleation is facilitated by a local inversion of the chemical profile. Normally, T_L increases with distance from the interface; however, compositional inhomogeneities can locally disturb this behavior, causing T_L to decrease ahead of the interface before increasing again farther into the liquid. This inversion favors the nucleation of new grains over growth of the existing solid, suppressing existing grains and enabling a fully equiaxed microstructure. In fact, columnar grains are completely absent at the bottom of the clad (Fig. 1*g*), where *G* is highest.

The proposed mechanism strongly depends on the solidification

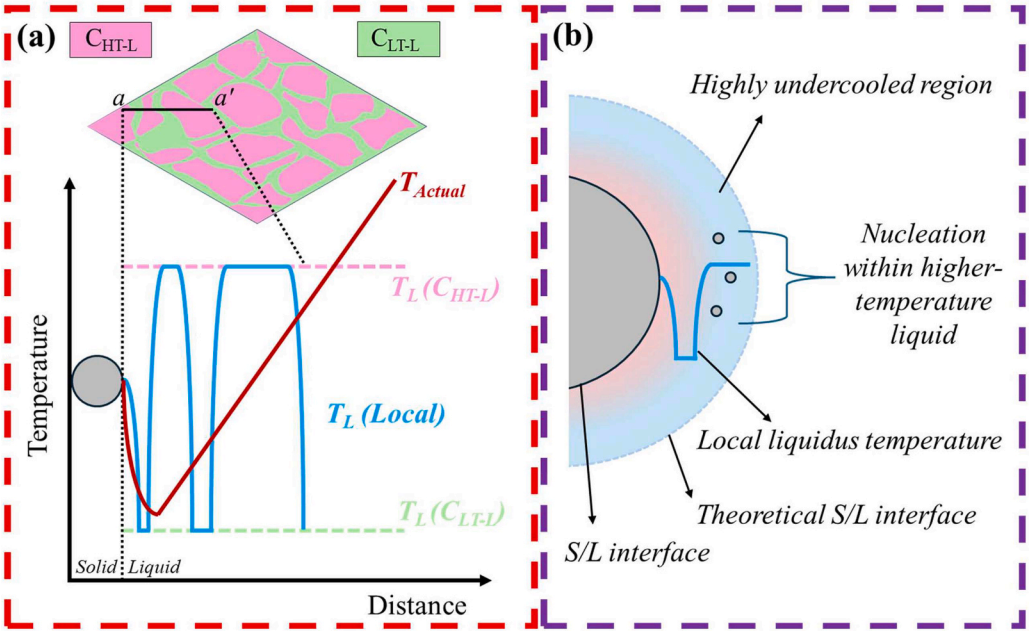

Fig. 2. Schematic illustration of the mechanism leading to complete CET in the MP-HEA: (a) spatial compositional fluctuations with higher-temperature ($C_{HT\text{-}L}$) and lower-temperature ($C_{LT\text{-}L}$) liquid regions, resulting in variations in the local liquidus temperature (T_L); (b) enhanced thermal undercooling ahead of the *S/L* interface caused by interface lag due to solute profile inversion, promoting nucleation in $C_{HT\text{-}L}$ regions.

temperature difference between the $C_{HT\text{-}L}$ and $C_{LT\text{-}L}$ regions (Fig. 3a). This difference (ΔT_c), arising from compositional variations, can be expressed as $\Delta T_c = m_a(C_{LT-L} - C_{HT-L})$, where m_a denotes the apparent liquidus slope, reflecting the non-equilibrium conditions. Consequently, the mechanism is highly sensitive to the magnitude of m_a. In the AlCoCrFeNi system, Al significantly influences m_a due to its low melting point, strongly negative enthalpies of mixing with transition metals [25], and low partition coefficient [26]. Higher Al content also increases local compositional differences, as melt mixing and homogenization become more difficult. Fig. 3b presents interfacial microstructures of CoCrFeNi, $Al_{0.3}$CoCrFeNi, and $Al_{0.7}$CoCrFeNi fabricated from mechanically mixed powders under identical laser conditions. While CoCrFeNi and $Al_{0.3}$CoCrFeNi still exhibit columnar grains, only a few fine columnar grains appear near the substrate in $Al_{0.7}$CoCrFeNi, confirming that Al increases ΔT_c via enhanced m_a and local compositional variations, enabling full CET in the AlCoCrFeNi MP-HEA.

Microstructural features within the melt pool are strongly affected by the combined effects of G and R, which vary throughout the melt pool due to different solidification conditions. As well established [27], higher cooling rates (i.e., higher GR) produce finer dendritic structures and smaller grains because the liquid undergoes greater ΔT, dominated by ΔT_t. This enhanced undercooling promotes nucleation while limiting grain coarsening. Near the substrate interface (bottom of the clad), intensified cooling increases nucleation, refining grains in this region of the MP-HEA. Accordingly, the size of the equiaxed grains grows with distance from the interface. Another contributing factor may be the varying extent of constitutional fluctuations. The upper melt pool, first to melt and last to solidify (except for the very top layer), experiences higher heat input and temperatures. Longer exposure to elevated liquid-state temperatures favors greater chemical homogenization, reducing ΔT_c, and combined with a lower ΔT_t from slower cooling, results in slightly coarser grains.

In the GP-HEA, on the other hand, with a homogeneous liquid composition, solidification is primarily determined by G and R. CET can thus be characterized by a critical G/R ratio, below which equiaxed grains are favored [17]. In this case, columnar grains dominate near the bottom of the clad, where G/R is high, while toward the top, decreasing G/R expands the constitutionally undercooled zone and triggers nucleation, transitioning from columnar to equiaxed morphology (Fig. 3c).

According to the Interdependence Theory [28], alloys with high Q values can rapidly develop substantial constitutional undercooling, activating many nucleant particles and thereby refining the grain structure [19,28]. For multicomponent alloys, $Q = \left(\partial \Delta T_{CS}/\partial f_s\right)_{f_s \to 0}$, where $\Delta T_{CS} = T_L - T_{Actual}$ and f_s is the solid fraction [29]. Scheil solidification curves for $AlCoCrFe_2Ni$ and $CoCrFe_2Ni$, calculated using compositions adjusted to the measured values (Table 1), are presented in Fig. 4a. As shown, Al addition significantly broadens the solidification range. From these curves and the equation above, the resulting Q values are ~101 °C for $AlCoCrFe_2Ni$ and ~3 °C for $CoCrFe_2Ni$ (Fig. 4b). Despite the high Q of $AlCoCrFe_2Ni$, equiaxed grains form only after the G/R ratio decreases in the GP-HEA. Moreover, these equiaxed grains are considerably coarser than those in the MP-HEA, highlighting the crucial role of constitutional fluctuations in enhancing ΔT and the nucleation rate compared with classical segregation-induced undercooling.

Notably, the observed grain-refining effect is comparable to that achieved with potent inoculants, suggesting that liquid constitutional fluctuations may serve as an intrinsic, self-generated inoculation mechanism. In conventional grain refinement, externally introduced particles act as preferential nucleation sites by reducing the local energy barrier (ΔT_n). Here, local compositional inhomogeneities perform a similar role by creating undercooled zones that serve as nucleation sites. Thus, even without foreign particles, the system internally generates conditions analogous to heterogeneous nucleation on inoculants, effectively refining the grain structure.

Direct observation of liquid constitutional fluctuations is extremely difficult, if not impractical. Nevertheless, indirect evidence is provided

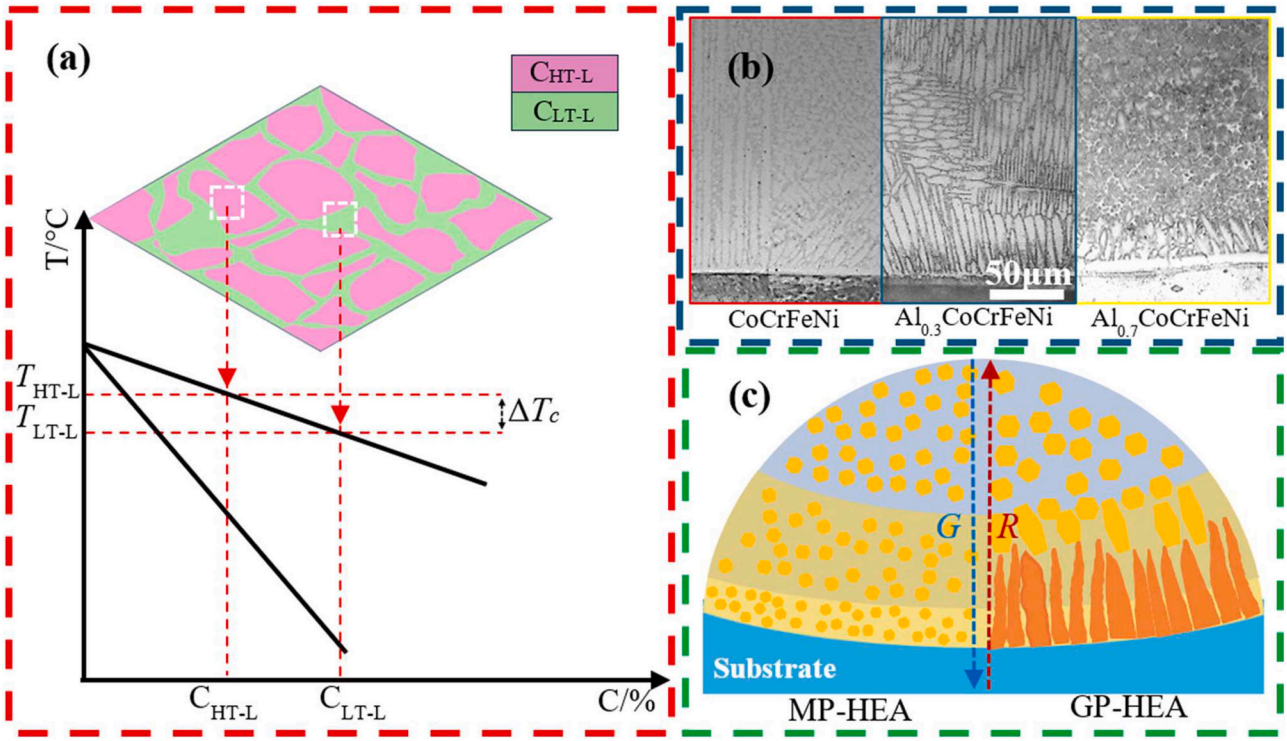

Fig. 3. Schematic and experimental evidence supporting the proposed CET mechanism in the MP-HEA: (a) difference in the liquidus temperature (ΔT_c) caused by liquid constitutional fluctuations; (b) optical images showing interfacial microstructures of laser-processed HEAs with varying Al content; (c) comparative representation of the MP-HEA and GP-HEA solidification behaviors. The arrow direction indicates how G (or R) decreases (or increases) from the bottom to the top of the clad, while the different colors in the melt pool correspond to distinct regions.

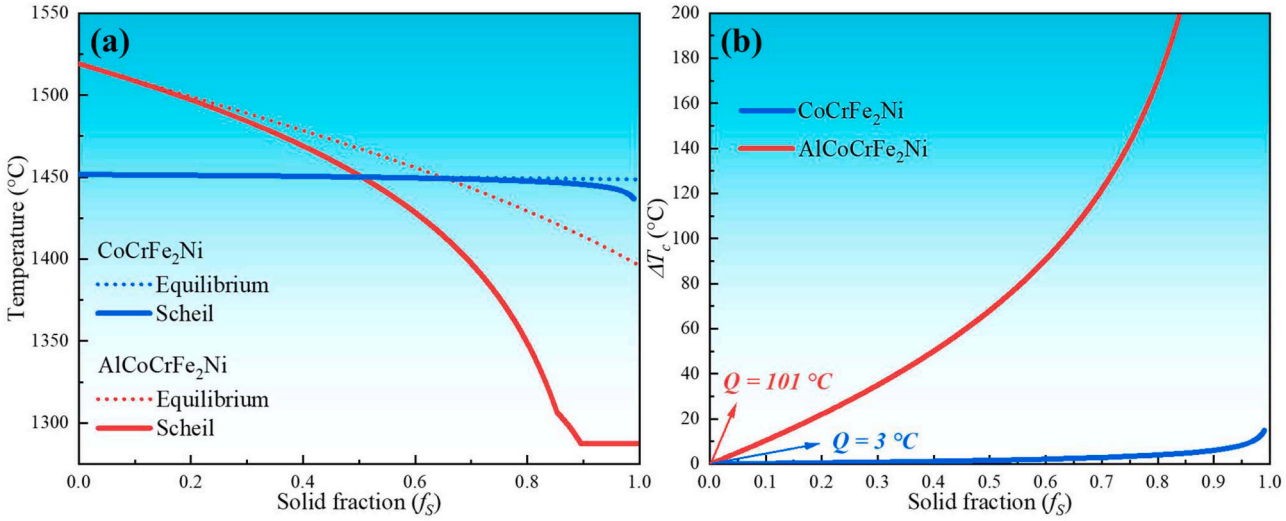

Fig. 4. (a) Scheil solidification curves and (b) constitutional undercooling as a function of solid fraction, derived from Scheil calculations and used to determine the growth restriction factor (Q) for the $AlCoCrFe_2Ni$ and $CoCrFe_2Ni$ HEAs (compositions adjusted to the measured values, as shown in Table 1).

by Fig. 5 and Table 2. The SEM image (Fig. 5a) and EDS maps (Fig. 5b) show that grain boundaries in the MP-HEA are decorated with Cr-rich precipitates. EDS point analyses at grain boundaries (region A) and grain interior (region B) (Table 2) further confirm significant compositional differences. In contrast, the GP-HEA exhibits markedly different behavior (Fig. 5(c-d)), with limited solute partitioning during solidification. Grain boundaries appear well defined due to metallographic preparation, but no precipitates are observed at the analyzed scale, and typical EDS point analyses (Table 2) corroborate the limited partitioning between regions C and D. Although anomalous segregation behavior has been previously reported in rapidly solidified alloys [30], both the MP- and GP-HEA samples in this study were processed under comparable solidification conditions. Under such circumstances, if the liquid in the MP-HEA was compositionally homogeneous prior to solidification, similar partitioning would be expected. While in-situ alloying may slightly influence thermal parameters, this alone is unlikely to account for the pronounced differences in solute partitioning. Furthermore, Fe contents in regions A and B of the MP-HEA (Table 2) are much lower than the average Fe content measured over a larger area (Table 1), which can only be rationalized by compositional heterogeneities in the liquid. Together, these observations consistently indicate a lack of chemical homogeneity in the liquid during solidification of the MP-HEA.

Table 2
Typical chemical compositions of different regions (Figs. 5a and 5c) in the as-solidified MP-HEA and GP-HEA determined by SEM-EDS.

Sample/Position		Composition (at. %)				
		Al	Co	Cr	Fe	Ni
MP-HEA	A	5.46	16.59	36.09	25.82	16.03
	B	19.18	19.00	12.29	29.90	19.63
GP-HEA	C	17.05	15.14	15.65	38.05	14.12
	D	17.01	15.45	15.81	36.41	15.32

Based on the proposed mechanism, controlling liquid constitutional fluctuations is essential for effective grain refinement without inoculants. The refined and nearly uniform microstructure in the MP-HEA

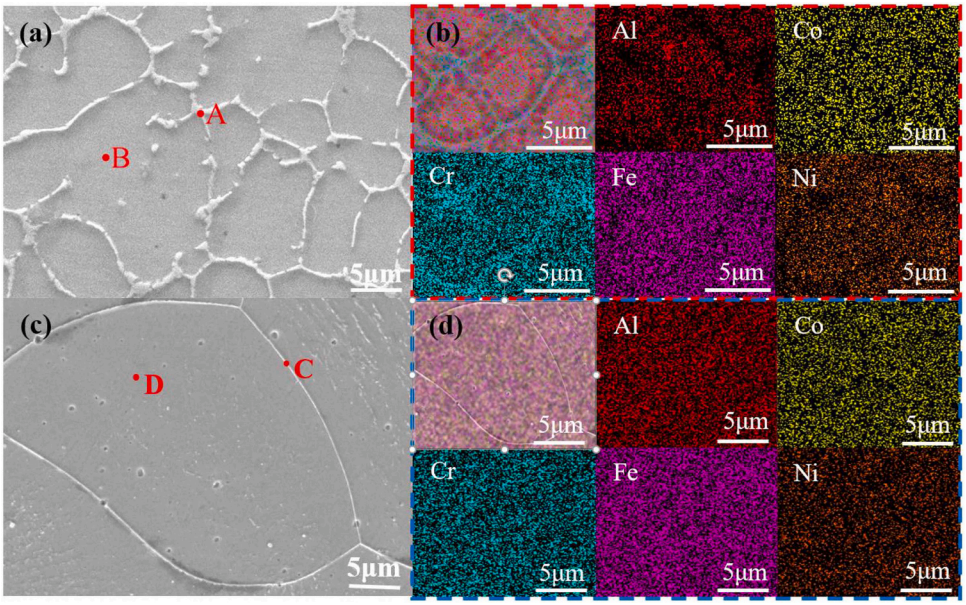

Fig. 5. Secondary-electron SEM images and EDS elemental maps of the as-solidified (a, b) MP-HEA and (c, d) GP-HEA.

is believed to originate from fine and well-distributed compositional variation fields (schematically shown in Fig. 2a). In this context, laser parameters, as well as powder size, morphology, and distribution, are expected to strongly influence the formation and evolution of these fields. Conditions that promote highly homogeneous liquids within the melt pool, such as very high energy densities, tend to suppress the mechanism. Conversely, excessively heterogeneous liquids produced under low energy conditions may generate coarse compositional gradients that also prevent uniform refinement. This latter behavior is commonly observed during in-situ alloying via LAM, where stratified compositional patterns lead to non-uniform nucleation and complex grain morphologies [31,32].

Powder feedstock variations have recently been explored as a means of deliberately introducing heterogeneities to tailor microstructural development in LAM [33,34]. For instance, Li et al [33] employed mixtures of powders with different compositions to generate controlled mesoscale chemical heterogeneities, promoting the formation of multiphase microstructures accompanied by pronounced variations in grain size and morphology. In-situ alloying studies demonstrate that grain morphology is highly sensitive to local chemical variations; however, the resulting compositional heterogeneities reported to date are typically coarse, leading to irregular microstructures [32,35]. In the present work, the results suggest that very fine and uniform grain structures can also originate from chemical heterogeneities in the liquid, provided that their magnitude and spatial distribution are favorable, as proposed here. Therefore, achieving suitable compositional fluctuations appears to be critical. These observations emphasize the need for systematic studies to elucidate the influence of raw materials characteristics and processing parameters on solidification and microstructural refinement.

In summary, this study reveals that a complete CET in laser-processed AlCoCrFeNi is governed not solely by thermal parameters and bulk composition but also by local chemical heterogeneities arising from powder composition. The use of mechanically mixed elemental powders may induce liquid constitutional fluctuations during solidification, locally inverting the solute profile and depressing the effective liquidus temperature ahead of the solid–liquid interface. This promotes intense undercooling and nucleation of new grains, suppressing the columnar front and producing a fully equiaxed microstructure. In contrast, pre-alloyed powders lead to conventional columnar growth dictated by the G/R ratio. Although direct observation of liquid-state compositional fluctuations was not feasible, the proposed mechanism consistently explains the experimental observations. These findings suggest that liquid constitutional fluctuations can act as an intrinsic, self-generated inoculation mechanism, enabling microstructural refinement without external additives. This concept provides a new pathway to tailor grain structure in laser-processed HEAs and other compositionally complex alloys, expanding the fundamental understanding of solidification under non-equilibrium conditions.

CRediT authorship contribution statement

Hui Zhang: Writing – review & editing, Supervision, Funding acquisition. **Yuyun Lu:** Writing – original draft, Investigation, Formal analysis. **Xueting Wu:** Writing – review & editing, Formal analysis. **Jingxi Zhang:** Writing – review & editing, Investigation, Formal analysis. **Dong Hao:** Writing – review & editing, Investigation, Formal analysis. **Ye Tao:** Writing – review & editing, Investigation, Formal analysis. **Lei Hu:** Writing – review & editing, Investigation, Formal analysis. **Dongzhen Qi:** Investigation. **Kaio Niitsu Campo:** Writing – review & editing, Validation, Formal analysis. **Sheng Guo:** Writing – review & editing, Validation, Formal analysis, Conceptualization.

Declaration of competing interest

The authors declare that they have no known competing financial interests or personal relationships that could have appeared to influence the work reported in this paper.

Acknowledgments

This work was financially supported by the National Natural Science Foundation of China (Grant No. 51971001). The Article Processing Charge (APC) for this publication was funded by the Coordination for the Improvement of Higher Education Personnel - CAPES (ROR: 00x0ma614). For open access purposes, the authors have assigned a Creative Commons CC BY license to any accepted version of the article.

Supplementary materials

Supplementary material associated with this article can be found, in the online version, at doi:10.1016/j.scriptamat.2026.117223.

References

[1] J.H. Martin, B.D. Yahata, J.M. Hundley, J.A. Mayer, T.A. Schaedler, T.M. Pollock, 3D printing of high-strength aluminium alloys, Nature 549 (2017) 365–369.
[2] J. Ren, Y. Zhang, D.X. Zhao, Y. Chen, S. Guan, Y.F. Liu, L. Liu, S.Y. Peng, F.Y. Kong, J.D. Poplawsky, G.H. Gao, T. Voisin, K. An, Y.M. Wang, K.Y. Xie, T. Zhu, W. Chen, Strong yet ductile nanolamellar high-entropy alloys by additive manufacturing, Nature 608 (2022) 62–68.
[3] J. Shittu, M. Sadeghilaridjani, M. Pole, S. Muskeri, J. Ren, Y. Liu, I. Tahoun, H. Arora, W. Chen, N. Dahotre, S. Mukherjee, Tribo-corrosion response of additively manufactured high-entropy alloy, Npj Mater. Degrad. 5 (2021) 31.
[4] M. Prost, A. Köster, D. Missoum-Benziane, S. Dépinoy, L. Ferhat, M. Rambaudon, V. Maurel, Anisotropy in cyclic behavior and fatigue crack growth of IN718 processed by laser powder bed fusion, Addit. Manuf. 61 (2023) 103301.
[5] D. Zhang, D. Qiu, M.A. Gibson, Y. Zheng, H.L. Frasier, D.H. StJohn, M.A. Easton, Additive manufacturing of ultrafine-grained high-strength titanium alloys, Nature 576 (2019) 91–96.
[6] V.P.N. Samy, M. Schäfle, F. Brasche, U. Krupp, C. Haase, Understanding the mechanism of columnar-to-equiaxed transition and grain refinement in additively manufactured steel during laser powder bed fusion, Addit. Manuf. 73 (2023) 103702.
[7] J.D. Hunt, Steady state columnar and equiaxed growth of dendrites and eutectic, Mater. Sci. Eng. 65 (1984) 75–83.
[8] A. Roy, A.K. Singh, A. Arora, B.A. McWilliams, C. Mock, K.C. Cho, R.S. Mishra, Columnar-to-equiaxed transition in laser fusion additive manufacturing, Scr. Mater. 259 (2025) 116565.
[9] D.J. Browne, A new equiaxed solidification predictor from a model of columnar growth, ISIJ Int. 45 (2005) 37–44.
[10] D.H. StJohn, A. Prasad, M.A. Easton, M. Qian, The contribution of constitutional supercooling to nucleation and grain formation, Metall. Mater. Trans. A 46 (2015) 4868–4885.
[11] L.L. Zhang, H.X. Jiang, J. He, J.Z. Zhao, A new model of growth restriction factor for hypoeutectic aluminium alloys, Scr. Mater. 179 (2020) 99–101.
[12] X.W. Liu, J.Q. Yao, X.N. Ma, Y.S. Wang, N. Gao, Y. Shi, Z.T. Fan, H. Du, Columnar-to-equiaxed transition and grain refinement by solute interaction effects, Mater. Charact. 205 (2023) 113288.
[13] Z. Fan, F. Gao, Y. Wang, H. Men, L. Zhou, Effect of solutes on grain refinement, Prog. Mater. Sci. 123 (2022) 100809.
[14] J.Q. Chang, Y.J. Ma, S.S. Huang, M. Qi, Z.R. Zhai, Y.N. Wu, R. Yang, Z.B. Zhang, Additive manufacturing of a new titanium alloy with tunable microstructure and isotropic properties, Addit. Manuf. 95 (2024) 104546.
[15] S.X. Wang, S.F. Li, X.M. Gan, R. Zheng, D. Ye, R.D.K. Misra, K. Kondoh, Y.F. Yang, Achieving synergy of mechanical isotropy and tensile properties by constructing equiaxed microstructure in as-printed Ti alloys, Scr. Mater. 229 (2023) 115379.
[16] K. Ma, Y.H. Cheng, N. Jeyaprakash, J.L. Zhou, Y.X. Wan, W.H. Yang, Temperature gradient and solidification rate simulation model of the microstructure of laser-cladded 27SiMn, Metals 13 (2023) 1682.
[17] M. Gäumann, C. Bezençon, P. Canalis, W. Kurz, Single-crystal laser deposition of superalloys: processing-microstructure maps, Acta Mater. 49 (2001) 1051–1062.
[18] M.N. Pater, D. Qiu, G. Wang, M.A. Gibson, A. Prasad, D.H. StJohn, M.A. Easton, Understanding the refinement of grains in laser surface remelted Al-Cu alloys, Scr. Mater. 178 (2020) 447–451.
[19] Q. Tan, Y. Yin, A. Prasad, G. Li, Q. Zhu, D.H. StJohn, M.-X. Zhang, Demonstrating the roles of solute and nucleant in grain refinement of additively manufactured aluminium alloys, Addit. Manuf. 49 (2022) 102516.
[20] R.T. Wang, H. Liu, P.J. Chen, X.H. Liu, J.B. Hao, H.F. Yang, Enhancing wear resistance of laser-clad AlCoCrFeNi high-entropy alloy via ultrasonic surface rolling extrusion, Surf. Coat. Tech. 485 (2024) 130908.
[21] I. Kunce, Marek Polański, K. Karczewski, Tomasz Płociński, K.J. Kurzydłowski, Microstructural characterization of high-entropy alloy AlCoCrFeNi fabricated by laser engineered net shaping, J. Alloys Compd. 648 (2015) 751–758.
[22] A.F. Andreoli, X. Han, I. Kaban, In situ studies of non-equilibrium crystallization of Al_xCoCrFeNi (x = 0.3, 1) high-entropy alloys, J. Alloys Compd. 922 (2022) 166209.

[23] W. Kurz, D.J. Fisher, Fundamentals of Solidification, 4th ed., Trans Tech Publications, Aedermannsdorf, Switzerland, 1998.
[24] A. Prasad, L. Yuan, P. Lee, M. Patel, D. Qiu, M. Easton, D. StJohn, Towards understanding grain nucleation under additive manufacturing solidification conditions, Acta Mater. 195 (2020) 392–403.
[25] A. Takeuchi, A. Inoue, Classification of bulk metallic glasses by atomic size difference, heat of mixing and period of constituent elements and its application to characterization of the main alloying element, Mater. Trans. 46 (2005) 2817–2829.
[26] G. Liu, L. Liu, X. Liu, Z. Wang, Z. Han, G. Zhang, A. Kostka, Microstructure and mechanical properties of $Al_{0.7}$CoCrFeNi high-entropy-alloy prepared by directional solidification, Intermetallics 93 (2018) 93–100.
[27] A.M. Sedighi, S.F. Nabavi, A. Farshidianfar, A review on effect of cooling rate on metallurgical, mechanical, geometrical characteristics and defects of laser cladding process, Lasers Manuf. Mater. Process. 11 (2024) 677–742.
[28] D.H. StJohn, M. Qian, M.A. Easton, P. Cao, The interdependence theory: the relationship between grain formation and nucleant selection, Acta Mater. 59 (2011) 4907–4921.
[29] M.A. Easton, D.H. StJohn, A model of grain refinement incorporating alloy constitution and potency of heterogeneous nucleant particles, Acta Mater. 49 (2001) 1867–1878.
[30] T. Mossop, D.J. Browne, M. Celikin, Anomalous solidification behaviour in rapidly cooled Ti-Nb-Ta ternary alloys, J. Mater. Res. Technol. 37 (2025) 260–267.
[31] J. Shinjo, A. Kutsukake, A. Arote, Y.T. Tang, D.G. McCartney, R.C. Reed, C. Panwisawas, Physics-based thermal-chemical-fluid-microstructure modelling of in-situ alloying using additive manufacturing: composition-microstructure control, Addit. Manuf. 64 (2023) 103428.
[32] S. Wei, P. Wang, L. Zhang, U. Ramamurty, Grain morphologies in additively manufactured alloys: from solidification fundamentals to advanced microstructure control, J. Mater. Sci. Technol. 235 (2025) 133–145.
[33] H. Li, S. Thomas, C. Hutchinson, Delivering microstructural complexity to additively manufactured metals through controlled mesoscale chemical heterogeneity, Acta Mater. 226 (2022) 117637.
[34] S. Chandra, C. Wang, S.B. Tor, U. Ramamurty, X. Tan, Powder-size driven facile microstructure control in powder-fusion metal additive manufacturing processes, Nat. Commun. 15 (2024) 3094.
[35] S. Chandra, J. Radhakrishnan, S. Huang, S. Wei, U. Ramamurty, Prog. Mater. Sci. 148 (2025) 101361.